IEEE Journal of Microwaves

Received 1 August 2022; revised 6 October 2022; accepted 27 November 2022. Date of publication 19 December 2022; date of current version 6 January 2023.

Digital Object Identifier 10.1109/JMW.2022.3225629

Quasi-Elliptical Stub-Based Multi-Resonance Waveguide Filters With Low Manufacturing Complexity for mm-Wave Applications

DANIEL MIEK (Member, IEEE), FYNN KAMRATH (Graduate Student Member, IEEE), KENNET BRAASCH, PATRICK BOE (Graduate Student Member, IEEE), AND MICHAEL HÖFT (Senior Member, IEEE)

(Regular Paper)

Department of Electrical and Information Engineering, Kiel University, 24143 Kiel, Germany

CORRESPONDING AUTHOR: Daniel Miek (e-mail: dami@tf.uni-kiel.de).

This work was supported by DFG within the funding program Open Access Publikationskosten.
This work did not involve human subjects or animals in its research.

ABSTRACT In this paper, the design and realization of quasi-elliptical waveguide filters with reduced manufacturing complexity are discussed. The filters are based on TE mode cavities, which are loaded with TM mode stubs. It is shown that dual-, triple- and quadruple-resonance segments are obtained by using up to three stubs loaded on the broad side of a TE mode cavity. The structures obtained can either be used as a stand-alone filter or even as a building block suitable for the realization of higher order filters. The multi-resonance blocks reveal several advantages in the mm-wave area: The manufacturing complexity is easy to handle and comparable to simple all-pole filters, which is especially important at high frequencies. Therefore, three prototypes are manufactured as proof of concept in the D-band (110 GHz–170 GHz). Moreover, the building blocks are able to produce $n-1$ transmission zeros (TZs) with n being the number of resonances. Therefore, the blocks generate between one (dual-resonance) and up to three (quadruple-resonance) TZs. Advantageously, the filters can be cut in the E-plane in order to reduce the insertion loss and hence consist of only two components. Three examples are manufactured by high precision CNC milling and reveal good agreement to the simulation by obtaining unloaded Q-factors of up to 1000.

INDEX TERMS D-band filter, E-plane cut, high precision CNC milling, reduced manufacturing complexity, TM mode stub.

I. INTRODUCTION

Waveguide components in the sub-terahertz frequency range are a current research topic due to the steadily increasing data rates in modern communication systems. This trend leads to a higher demand for bandwidth resources, which can be met especially at high carrier frequencies. While in the lower gigahertz regime versatile technologies are known for the realization of microwave filters (e.g. microstrip, coaxial or dielectric), in the mm-wave area the focus usually lies on the waveguide technology. The manufacturing of waveguide components in the lower frequency bands is generally not associated with any difficulties and different manufacturing techniques are available, including the classical computerized numerical control (CNC) milling or versatile 3-D printing approaches [1], [2]. Up to moderate center frequencies, tuning screws might be used to compensate for manufacturing tolerances.

The requirements and hence the manufacturing techniques change when the center frequency is further increased. For example, in the mm-wave frequency range tuning of the components is almost not possible anymore, leading to the need of an inherent high manufacturing accuracy. Consequently, it is important that the structures to be realized are in harmony with the manufacturing approach to mitigate this problem and reduce the reject rate in the production of these components. Apart from CNC milling, the deep reactive ion etching (DRIE) approach as well as the SU-8 photoresist technique have proven to be suitable for the

realization of filters up to the terahertz regime [3], [4], [5]. In both approaches, individually structured layers are stacked above each other. In case of DRIE, TM dual-mode filters have proven to be well suited for this manufacturing approach [6], [7], [8]. Especially, small coupling elements can be manufactured with high precision. A similar statement is valid for the SU-8 photoresist technique, where cascading several layers leads to good results [9], [10], [11]. A disadvantage of both approaches is that specialized holders for measurement and mounting might be required. In addition, the machines for the production of both technologies are not as commonly used as high precision CNC milling machines.

Implementing microwave filters by using multiple parts is not meaningful if the milling approach is used for fabrication. A high number of individual parts leads to inherent increased losses because of the finite surface roughness and tolerances arise due to the alignment of the parts. Considering the CNC milling process, the component to be realized should consist of ideally only two individual parts. This reduces alignment problems as well as electrical losses. To further account for the last aspect, an E-plane cut is highly desirable. All-pole filters with an E-plane cut were already published in the literature with remarkable performance [12], [13], [14]. Nevertheless, no finite transmission zeros (TZs) are available to increase the filter selectivity. This property is, however, highly desirable in order to efficiently fulfill the rejection requirements while keeping the filter order as small as possible. Filters with finite TZs are in many cases realized with an H-Plane cut, e.g. [15], [16], [17], [18]. These filters are either implemented as a classical quadruplet topology or utilize the singlet approach [19], [20], [21]. In many cases the filters resulting from these design approaches do not reveal an E-plane symmetry.

To improve this circumstance, this paper presents multi-resonance building blocks consisting of a TE mode cavity which is loaded with up to three TM mode E-plane stubs. These segments are well-suited for the CNC milling approach especially in high frequency bands due to the following reasons:

- The filters are symmetric and therefore allow the implementation of an E-plane cut to improve the manufacturing quality as well as to reduce the insertion loss.
- The filters are easy to fabricate as there are no structures that are difficult to realize such as capacitive gaps or cavities with high aspect ratio. Furthermore, alignment issues are reduced to a minimum as only two parts are required.
- A cavity loaded with stubs allows the implementation of the same number of finite TZs as the number of stubs used. Therefore, quasi-elliptical filter responses can be realized. The filter order can therefore be reduced as rejection specifications might be efficiently realized.

The article proposed here extends our basic investigations in [22]. The approach using stub-loaded cavities is primary based on the stubbed waveguide principle discussed in [23] and [24], where a TE_{201} mode cavity with one or optionally two E-plane stubs is used to realize highly compact filters at moderate frequencies (around 21 GHz as well as 31 GHz). The position of the stubs as well as the offset of the input / output coupling prevents the filters, however, to be realized with an E-plane cut. A similar statement is valid for the approach proposed in [25], where a dual-mode base-cavity is used and loaded with TM mode stubs to realize a pair of real frequency axis or even complex TZs. The approaches discussed there reveal several advantages with respect to size and weight reduction of the filters, however, the manufacturing complexity is not optimal for the realization in the mm-wave range (above 100 GHz).

Another interpretation of the structures proposed here is given by assuming the stubs as a dispersive admittance inverter. By using impedance as well as admittance inverters in a filter, the cavities between two different types of inverters need to be a quarter wavelength long instead of half a wavelength [26], [27], [28]. The arising TZ is then generated by the dispersive characteristic of the inverter realized by the stub. However, as the former interpretation of the stubs as TM mode resonators reveals several advantages by discussing the electrical filter behavior, this interpretation is used throughout the paper.

Based on the concepts in [23], [24], [25] and in extension to [22], this paper proposes quasi-elliptical waveguide filters based on the stub-approach. The focuses lie on an easy fabrication at mm-wave frequencies and the realization by high-precision CNC milling.

A TE_{101} / TE_{102} / TE_{103} mode cavity is loaded with one / two / three TM mode E-plane stubs, respectively, while each stub implements one reflection zero as well as one TZ. Depending on the filter set-up, the position of the TZs is either flexible or almost fixed. However, in the latter case, a certain flexibility is achieved by combining several of the proposed structures with non-resonating nodes (NRNs).

This paper is organized as follows: Section II provides an overview over the basic second order building block. The fields of the resonant modes as well as coupling matrix dependencies are discussed. The high design flexibility is proven on a fourth order filter realized by coupling two second order building blocks with a quarter wavelength coupling aperture. Basic design rules are discussed. A filter is designed and manufactured as proof of concept. Section III extends the principle to a TE_{102} mode base cavity loaded with two E-plane stubs. The resulting third order filter reveals a high design flexibility as well. A sixth order filter as a result of coupling two third order building blocks is manufactured. Section IV provides a further extension to a quadruple-resonance segment, consisting of a TE_{103} mode base cavity and three TM mode stubs. In Section V a comparison of the results obtained here with results from the literature is accomplished. Finally, Section VI summarizes and concludes this paper.

II. DUAL-RESONANCE SEGMENT

A. BASIC CONSIDERATIONS

The basic dual-resonance element is shown in Fig. 1. It consists of a TE_{101} mode cavity with length l_{cav}, width a

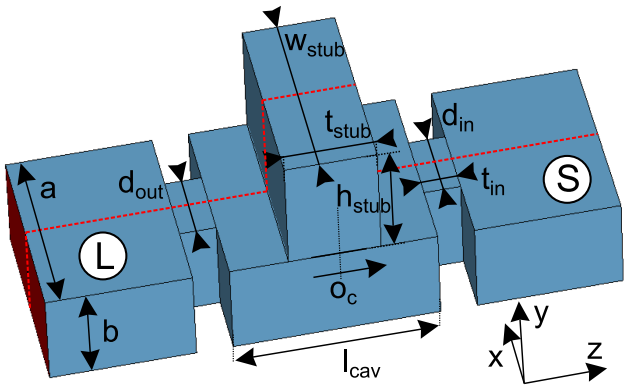

FIGURE 1. Dual-resonance element consisting of a main cavity with length l_{cav} and an E-plane TM mode stub. The red (dashed) line indicates the cutting plane. The waveguide dimensions are $a = 1.651$ mm and $b = 0.8255$ mm.

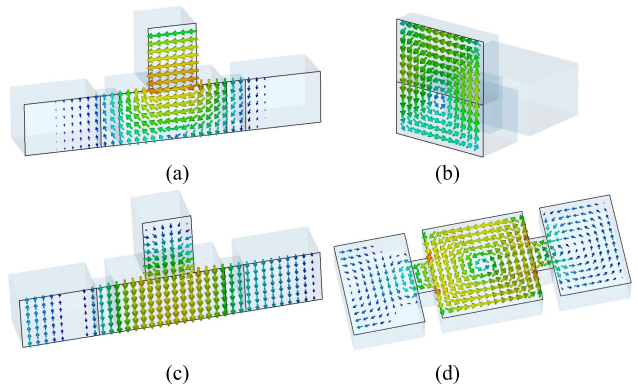

FIGURE 3. Field distribution at the resonance frequencies from Fig. 2: (a) and (b) electric / magnetic field distribution of TM_{110} mode (115.3 GHz); (c) / (d) electric / magnetic field distribution of TE_{101} mode (124.2 GHz).

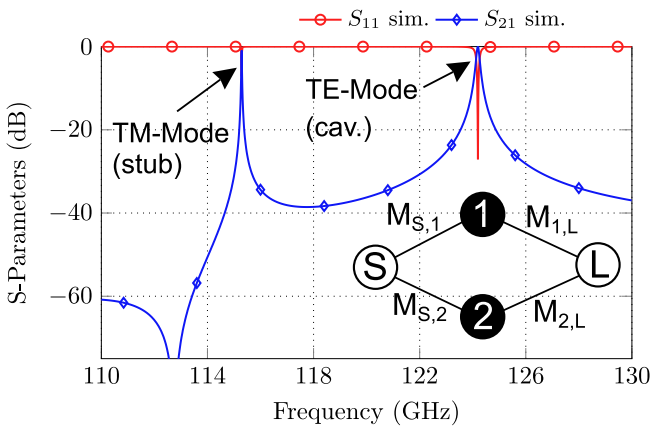

FIGURE 2. S-Parameter simulation of the resonator in Fig. 1 with weak excitation. The dimensions are chosen as follows (all in mm): $d_{in} = d_{out} = 0.6$, $l_{cav} = 1.7$, $h_{stub} = 1$, $t_{stub} = 0.756$, $t_{in} = 0.3$, $o_c = 0$, $w_{stub} = a$. The inset shows the topology of the dual-resonance element.

and height b (width and height of WR-6 waveguide standard, respectively) as a base. On top of the cavity, a TM mode stub with height h_{stub}, thickness t_{stub} and width w_{stub} is placed. The stub is centered with respect to the TE_{101} mode cavity and may have an offset in z-direction, which is denoted as o_c. The dual-resonance segment is coupled by inductive irises with diameter d_{in} and d_{out} to the in- and output, respectively. The red (dashed) line illustrates the E-symmetry plane, in which all filters within this paper can be cut for manufacturing purposes.

In a first investigation, the resonator is simulated with weak excitation ($d_{in} = d_{out} = 0.6$ mm) in order to evaluate the field distribution of the participating modes. The S-Parameters are shown in Fig. 2. One TZ at 112.74 GHz as well as two resonances can be observed. Fig. 3 shows the electric and magnetic field distribution at the resonance frequencies of the S-Parameter response in Fig. 2. The electric / magnetic fields of the lower-frequent mode at 115.3 GHz are shown in Fig. 3(a) and (b), respectively, which can be identified as a mode similar to TM_{110}. The field distribution of the resonance at 124.2 GHz is shown in Fig. 3(c) and (d) and is denoted as TE_{101} mode. In comparison to the "classical" TE_{101} mode, there are additional field portions within the stub. As no coupling element is located in the dual-resonance structure, both modes are excited from the source / load port. The corresponding coupling scheme is a transversal array of second order as shown in the inset of Fig. 2 [29]. The existence of the TZ in Fig. 2 can for example be explained by the electric field distribution of both resonant modes in Fig. 3(a) and (c). On the one hand, the field of the TE_{101} mode reveals the same direction at the input and output port, while the field of the TM_{110} mode exhibits an opposite direction at the ports. Therefore, one coupling factor in the transversal array must be interpreted negative. One the other hand, as can be seen in the field distributions in Fig. 3, the coupling strength between the source / load port and both resonating modes is different as required for the realization of a TZ.

By proper dimensioning, the dual-resonance segment can be tuned to realize a second order filter with one TZ. It is worth mentioning that the TZ can be flipped from one side of the passband to the other by exchanging the resonance frequencies of the resonating modes (zero shifting property) [30]. The dual-resonance segment is especially suitable for the derivation of coupling factor dependencies, which is convenient for the design of higher order filters. For this investigation, the dual-resonance element is matched to a return loss of $RL = 20$ dB between the band edges at $f_l = 117.27$ GHz and $f_u = 119.72$ GHz and thereby reveals one TZ below the passband at a normalized frequency of $f_{TZ,LP} = -j2.63$ (115.31 GHz). The normalized coupling factors are given as $M_{S,1} = M_{1,L} = 0.58$, $-M_{S,2} = M_{2,L} = 1.148$, $M_{1,1} = 1.6$ and $M_{2,2} = -1.41$ [29]. The dimensions of the prototype are found as (all in mm): $d_{in} = d_{out} = 1.02$, $t_{in} = 0.3$, $l_{cav} = 1.38$, $h_{stub} = 0.941$, $t_{stub} = 0.8$, $o_c = 0$ and $w_{stub} = a$.

Subsequently, the geometric dimensions are varied in discrete steps and the coupling matrix is extracted for each step.

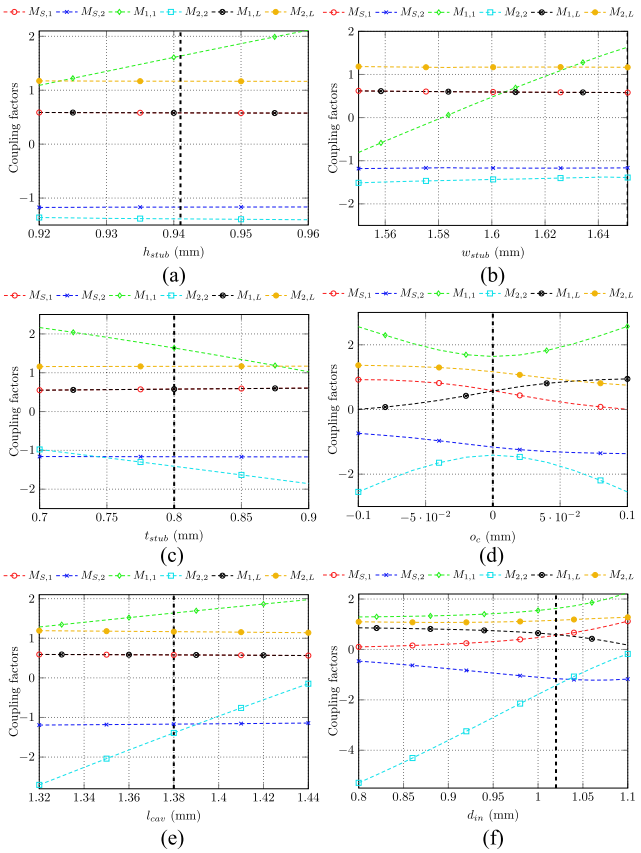

FIGURE 4. Dependencies of the coupling factors of a second order filter in transversal array topology upon geometric dimensions (compare Fig. 1). The vertical dashed lines visualize the ideal dimensions for which the filter is matched.

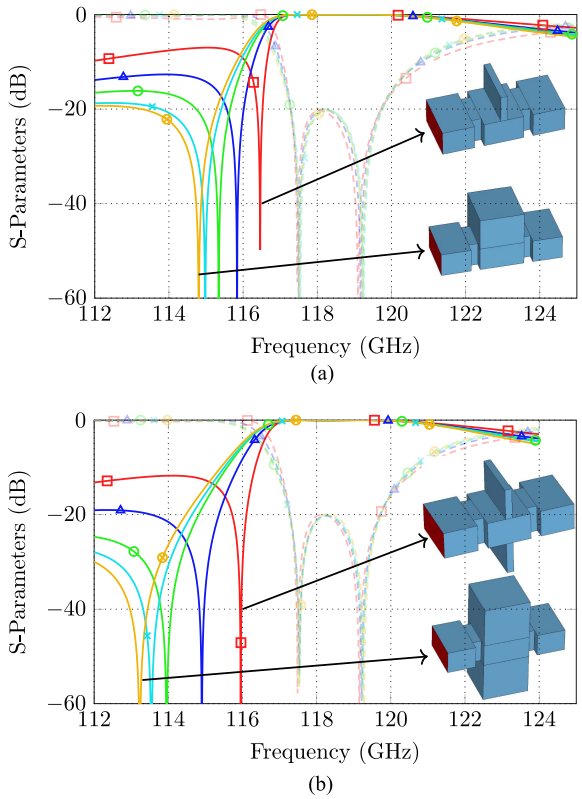

FIGURE 5. S-Parameter results of TZ study for: (a) second order building block with stub extending in one direction and (b) second order building with stub extending in both directions. The insets show the simulation set-ups of the borderline cases.

The results are shown in Fig. 4. The vertical dashed lines visualize the dimensions, for which the filter is matched and fulfills the desired specifications. Fig. 4(a) shows the dependency of the coupling factors from the stub height h_{stub}. Obviously, only the coupling factor $M_{1,1}$ increases for an increasing stub height. This coupling factor might therefore be associated with the TM_{110} mode in the stub. A similar statement is valid for the variation of the stub width w_{stub} in (b), which might only be choosen smaller or identical to the waveguide width a due to manufacturing reasons. Apart from a neglectable variation in $M_{2,2}$, $M_{1,1}$ strongly depends on the stub width. As can be seen in (c), for the simulated parameter range an increase of the stub thickness t_{stub} leads to an increased center frequency as both self couplings $M_{1,1}$ and $M_{2,2}$ decrease. An offset from the center position of the stub o_c as well as a variation of the blend aperture diameter d_{in} should be used for an adaption of the coupling strength between the ports and the resonant modes. As an interesting observation, a shift of the stub leads to a decreasing coupling factor $M_{S,1}$ if it is shifted into the direction of the source port (an identical case occurs if the stub is shifted in the direction of the load port, where $M_{1,L}$ decreases). Furthermore, loading effects on both resonances can be identified by varying o_c or d_{in}. Please note, that varying o_c is only important for higher order filters as any transversal coupling matrix of second order requires $|M_{S,1}| = |M_{1,L}|$ and $|M_{S,2}| = |M_{2,L}|$ to realize a matched filter response, which is only fulfilled for $o_c = 0$ (cross-point of $M_{S,1}$ and $M_{1,L}$). Finally, from Fig. 4(e) one can conclude that the self coupling $M_{2,2}$ (TE_{101} mode) should be controlled by the length of the cavity l_{cav}, since the coupling factor $M_{1,1}$ can be compensated using w_{stub} and h_{stub}. Similar coupling factor dependencies can be observed, if a symmetric second order filter (where the stub extends in both directions) is investigated. From Fig. 4 it follows, that the TZ generated by the dual-resonance segment can either be positioned above or below the passband by exchanging the frequencies of both resonant modes.

Under the defined constraints and design variables, the relative position of the TZ can be varied to some extent by changing e.g. the stub thickness, which defines the only degree of freedom in the second order segment. A study is shown in Fig. 5(a). In this analysis, the stub thickness is enforced to a certain value and the filter is matched using the remaining geometrical parameters to maintain the same filter characteristic (band edges and return loss level). As a result, a minimal TZ position of $f_{TZ,LP,min} = -j1.68$ for a stub thickness of $t_{stub} = 0.2$ mm can be achieved. The maximal TZ position is achieved if the stub thickness is identical to the length of the

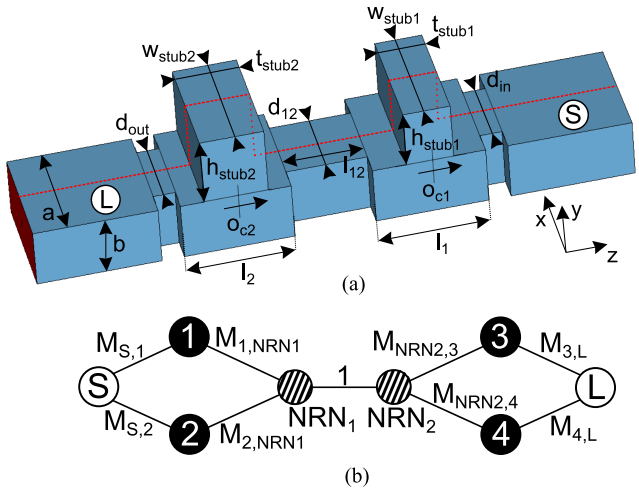

FIGURE 6. (a) Simulation model of a fourth order filter consisting of two second order segments coupled by a quarter wavelength inverter and (b) corresponding coupling topology.

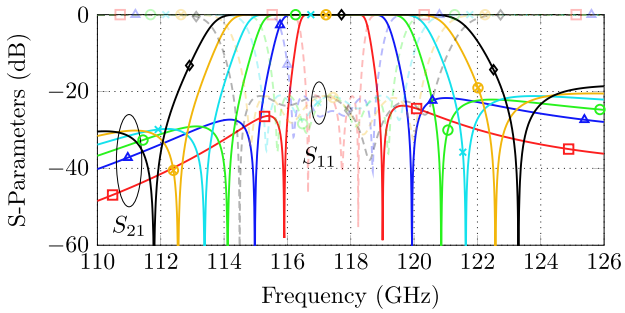

FIGURE 7. Bandwidth study of the fourth order filter as shown in Fig. 6(a). The bandwidth is varied between 1.7 GHz ($FBW = 1.45\%$) and 6.3 GHz ($FBW = 5.37\%$) while maintaining constant (symmetric) relative TZ positions.

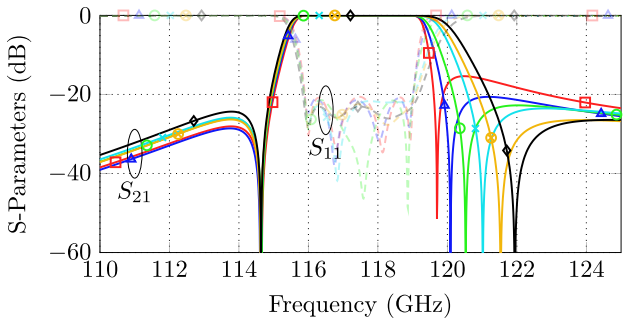

FIGURE 8. Flexibility of the upper TZ of the fourth order filter as shown in Fig. 6(a). The TZ is varied on the normalized frequency axis between $f_{TZ,LP} = j1.45$ (119.7 GHz) and $f_{TZ,LP} = j2.85$ (121.95 GHz).

base cavity. In this case the TZ occurs at a normalized frequency of $f_{TZ,LP,max} = -j3.07$. A similar statement is valid for the second order filter using a symmetric stub extending in both directions (compare insets in Fig. 5(b)), where the TZ can be placed at $f_{TZ,LP,min} = -j2.11$ for $t_{stub} = 0.2$ mm and $f_{TZ,LP,max} = -j4.42$ for $t_{stub} = l_{cav} = 1.63$ mm. The results in terms of S-Parameters are shown in Fig. 5(b). This paper focuses on filters realized by stubs extending in only one direction, while stubs extending symmetrically are used in filter design as well [25], [31]. A similar design flexibility as provided by the second order segment is realized by a fourth order filter as described in Sections II-B.

B. HIGHER ORDER FILTER DESIGN AND COUPLING MATRIX DESCRIPTION

A fourth order filter can be realized by cascading two second order segments with an iris aperture, whose length l_{12} is approximately a quarter wavelength at the filter center frequency. The simulation model is shown in Fig. 6(a) while one feasible coupling topology is depicted in (b). In the coupling matrix description, the iris aperture between both dual-resonance segments might be modeled as two consecutive NRNs, which are coupled by a unity inverter. The value of the self-couplings of both NRNs is set to zero in this case [21], [32], [33]. As the coupling inverter has a length of approximately a quarter wavelength, this seems to be a physically more meaningful description than the one initially proposed in [22], where only one NRN is placed in the coupling scheme to couple both cavities. Furthermore, the simulated S-Parameters might be modeled more precisely by utilizing this approach. As proof of this topology, the S-Parameters of the manufactured filter are compared with the simulation as well as the coupling matrix representation in Sections II-C.

Initial dimensions of a fourth order filter with one TZ below and one TZ above the passband can be obtained by cascading two second order segments as discussed in Sections II-A, where the dimensions of a second order filter with a TZ below the passband are given as well. The TZ can be flipped to the other side of the passband by choosing the dimensions of the cavity and stub to e.g. $l_{cav} = 1.524$ mm and $h_{stub} = 0.791$ mm, respectively, while maintaining all other dimensions. The coupling aperture between both dual-resonance segments is chosen with the initial dimensions $d_{12} = 1.05$ mm and $l_{12} = 1$ mm. The final dimensions for the desired bandwidth / TZ positions can efficiently be obtained by using for example the trust region framework optimization algorithm in CST Microwave Studio.

The flexibility of the proposed fourth order filter is represented in terms of Figs. 7 and 8. In Fig. 7 a bandwidth study is carried out. The center frequency is maintained constant at approximately 117.4 GHz while the bandwidth is varied between 1.7 GHz ($FBW = 1.45\%$) and 6.3 GHz ($FBW = 5.37\%$). The relative position of the TZs is choosen symmetrically at $f_{TZ,LP} = \pm j1.82$ and is constant within the framework of this study. Due to multiple cross-dependencies of the coupling factors as discussed in Fig. 4, the results of the bandwidth study are based on optimizing the structure in Fig. 6(a). Please note, that in the simulation model the upper TZ is generated by the generally smaller stub (characterized by l_1 and h_{stub1}) while the TZ below the passband is generated by the second stub. In addition to the optimization strategy, some basic dependencies observed by obtaining the presented

results might be identified. For example, for increasing the bandwidth, all coupling apertures (d_{in}, d_{12} and d_{out}) tend to enlarge as is commonly known for waveguide filters. Additionally, the length of the base cavities l_1 and l_2 needs to be reduced for increasing bandwidths. The height of the first stub (h_{stub1}) decreases for larger bandwidths while the height of the second stub (h_{stub2}) increases. This is expected as well, because the absolute positions of the TZs diverge for larger bandwidths.

Fig. 8 shows a TZ study, where for a given center frequency of approximately 117.44 GHz and bandwidth of 3.1 GHz the lower TZ is fixed at a normalized frequency of $f_{TZ,LP} = -j1.836$ (114.63 GHz) while the position of the upper TZ is varied. Within the framework of this study, the TZ is varied between $f_{TZ,LP} = j1.45$ (119.7 GHz) and $f_{TZ,LP} = j2.85$ (121.95 GHz). Even if a direct synthesis strategy is not available, some basic dependencies as in the case of the bandwidth study might be identified. One key element are the offsets o_{c1} and o_{c2}, which can be used to control the coupling strength from the source / load port to the TM_{110} modes in both stubs (compare Fig. 4(d)). Additionally, the input coupling strength d_{in} as well as the inter-cavity coupling d_{12} increases when shifting the TZ away from the passband. It is further worth mentioning that the thickness of the first stub t_{stub1} tends to decrease while shifting the TZ in the direction of the passband, which may lead to unrealistically small values (unpractical for manufacturing).

Different higher-order filter topologies can be obtained by combining either several dual-resonance segments or even by combining them with TE_{101} single-mode cavities. The flexibility in freely adapting the TZ positions by maintaining the overall filter characteristic can only be confirmed for the coupled fourth order filter presented in Fig. 6(a) as well as for the triple resonance segment presented in Section III. However, a certain degree of flexibility in case of higher order filters can be obtained by varying e.g. the positions of the dual-resonance segments within a filter. Furthermore it is possible, that any available TZs are flipped to an arbitrary side of the passband. Three examples will be discussed within the framework of Figs. 9–11.

In Fig. 9 the set-up of two different sixth order filters as well as simulated S-Parameter results are proposed. In Fig. 9(b) the dual-resonance segments are placed near to the source and load ports, respectively, while two TE_{101} mode cavities are placed in the filter center. The filter topology is abbreviated as "D-S-S-D," where "D" stands for dual- and "S" for single-resonance resonator. Within the framework of this study, two S-Parameter results with different bandwidths of $B_{min} = 2$ GHz and $B_{max} = 3.6$ GHz are shown. In order to obtain a matched filter response, the TZs arise at a normalized frequency of $f_{TZ,LP,Bmin} = \{-j2.09, j1.99\}$ in case of a bandwidth of 2 GHz and $f_{TZ,LP,Bmax} = \{-j1.88, j2.08\}$, if the bandwidth is tuned to 3.6 GHz. By considering the dual topology denoted as "S-D-D-S," where the dual-resonance segments are located in the filter center and the single-mode cavities are placed at the filter in- and output ports, the

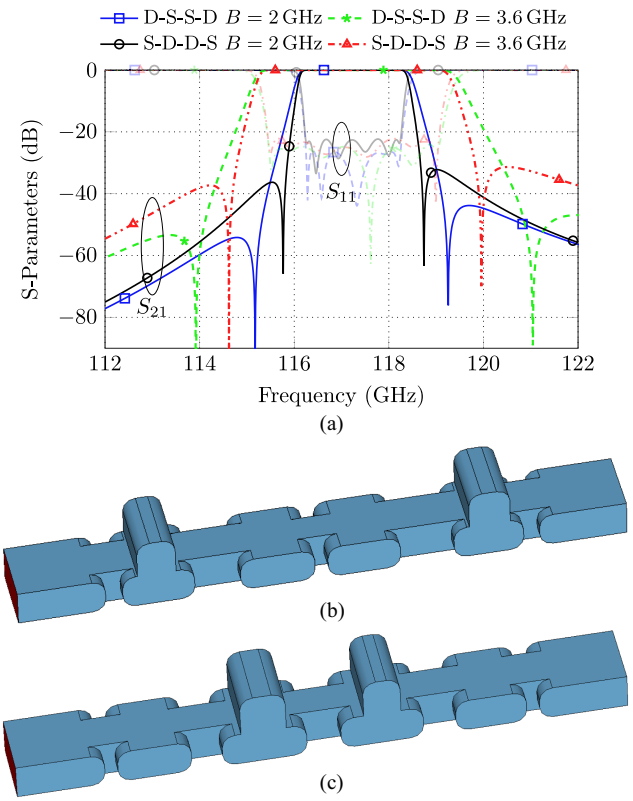

FIGURE 9. (a) Simulated S-Parameter results of the filters presented in (b) and (c), "D" stands for dual-resonance and "S" for single-resonance. (b) D-S-S-D filter set-up, (c) S-D-D-S filter set-up.

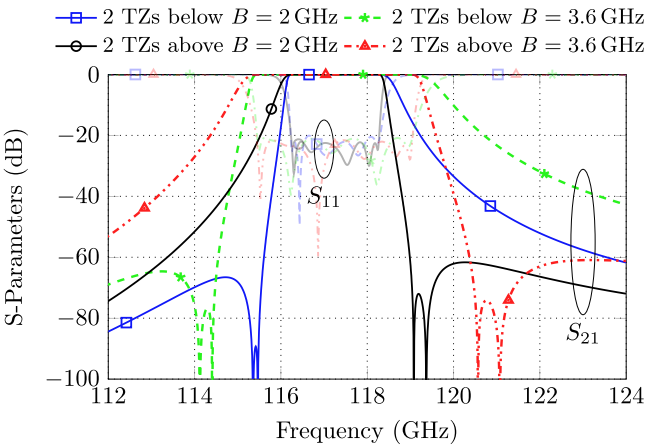

FIGURE 10. Simulated S-Parameter results of the filter from Fig. 9(b) with either both TZs above or below the passband and different bandwidth configurations.

TZs arise obviously closer to the passband at normalized frequencies $f_{TZ,LP,Bmin} = \{-j1.49, j1.49\}$ and $f_{TZ,LP,Bmax} = \{-j1.42, j1.41\}$.

Additional flexibility can be achieved by tuning e.g. both dual-resonance segments in a way, that the TZs arise at the same side nearby the passband. Simulated S-Parameter results for the filter set-up in Fig. 9(b) are shown in Fig. 10. The filters are again tuned to realize two different bandwidth

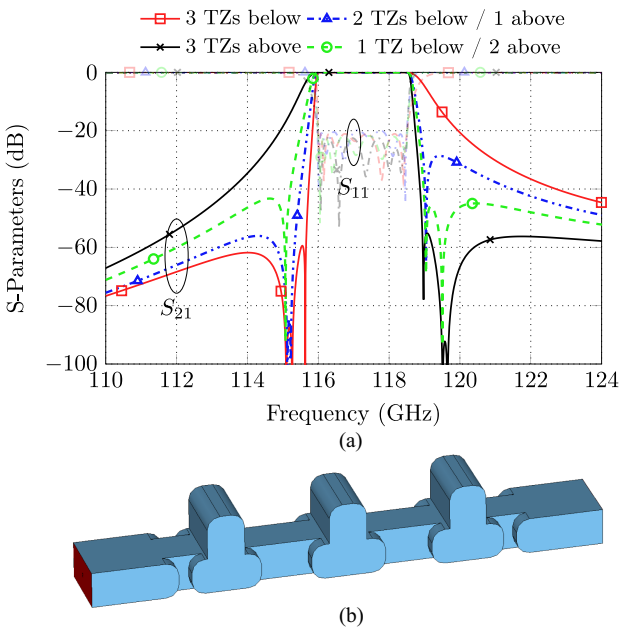

FIGURE 11. (a) Sixth order filter responses obtained by cascading three dual-resonance sections and (b) corresponding filter set-up.

configurations while both TZs arise either below or above the passband.

In Fig. 11(b) the simulation model of a sixth order filter consisting of three dual-resonance sections is shown. The coupling between the resonators is realized by apertures whose lengths are approximately a quarter wavelength. As each dual-resonance segment contributes two reflection and one transmission zero, a sixth order filter with three TZs is generated. It is easily possible to account for desired rejection specifications by flipping an arbitrary number of TZs either below or above the passband, which can be done by primarily varying the height of the individual stubs. Especially interesting is the possibility that all TZs can be placed above / below the passband. Combinations where two TZs are located below the passband and one TZ is above or vice versa are realizable as well. The S-Parameter responses are shown in Fig. 11(a). Similar specifications of a center frequency of 117.25 GHz and a bandwidth of 2.5 GHz are defined for each simulation.

C. MANUFACTURING AND MEASUREMENT RESULTS

In order to verify the good manufacturing properties of the proposed structures with respect to the milling technique, a fourth order filter according to the simulation model in Fig. 6 is manufactured as proof of concept. As discussed in [22], basically two cutting planes, which are required for the manufacturing, are available. On the one hand, the filter can be manufactured as a quasi H-plane cut, where both stubs are processed in one filter half and the remaining structure is manufactured in the other half. However, this approach is disadvantageous in terms of manufacturing accuracy and losses [22]. Surface currents flowing over the cutting plane reduce the unloaded quality factor while additionally the stubs

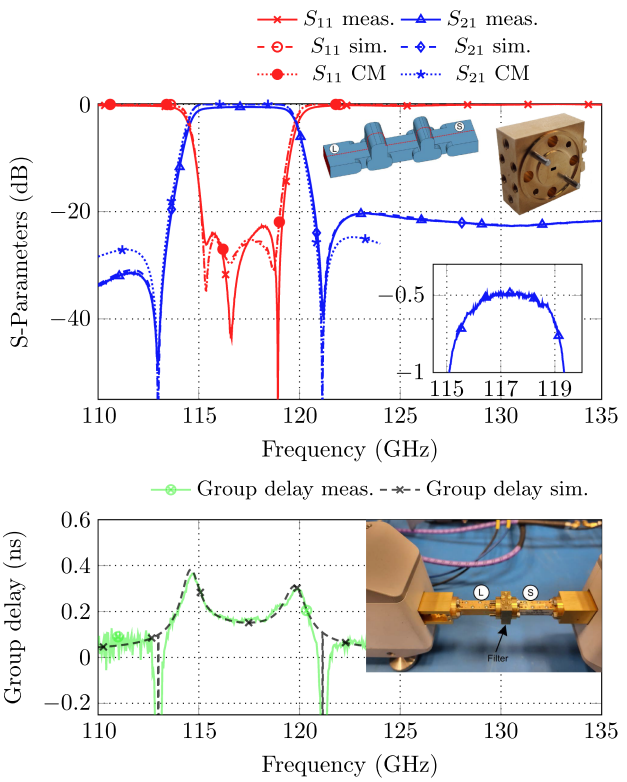

FIGURE 12. Top: Measurement results of the manufactured fourth order filter in comparison to the simulation and the coupling matrix representation. The insets show the simulation model with all required radii as well as the manufactured prototype. The coupling coefficients (with respect to Fig. 6(b)) are as follows: $M_{S,1} = -0.963$, $M_{S,2} = 0.65$, $M_{1,NRN1} = 1.033$, $M_{2,NRN1} = 0.435$, $M_{1,1} = 0.65$, $M_{2,2} = -1.28$, $M_{NRN2,3} = 0.298$, $M_{NRN2,4} = -0.742$, $M_{3,L} = 0.727$, $M_{4,L} = 1.04$, $M_{3,3} = 1.276$, $M_{4,4} = -0.887$. Bottom: Comparison of measured and simulated group delay. Inset: Measurement set-up.

might be difficult to manufacture (high aspect ratio). On the other hand, due to these reasons, the E-plane cut is the preferred choice for the manufacturing with the CNC milling approach. The adapted filter model including all radii as well as the used cutting plane is shown in the inset of Fig. 12. As a cutter with diameter of $d_c = 0.6$ mm is used, the radii are chosen to $r = 0.3$ mm. The radii in the stubs increase the frequency of the corresponding TM mode, which must be compensated by adapting the stubs height. A similar statement is valid for the base TE mode cavity, whose center frequency should be adjusted by varying the corresponding cavity length. The filter is designed to have the band edges at $f_l = 115.2$ GHz and $f_u = 119$ GHz while revealing a 25 dB return loss level. The filter is made from brass due to the good machining properties of this material. The measurement results show very good agreement with the simulation as is seen in Fig. 12. The return loss level is decreased to 22 dB due to manufacturing tolerances. The unloaded quality factor is determined by coupling matrix extraction methods [34] and can be estimated to be $Q_u \approx 830$. The filter (as well as all other prototypes presented here) are manufactured with a high precision CNC milling machine (Roeders RXP400).

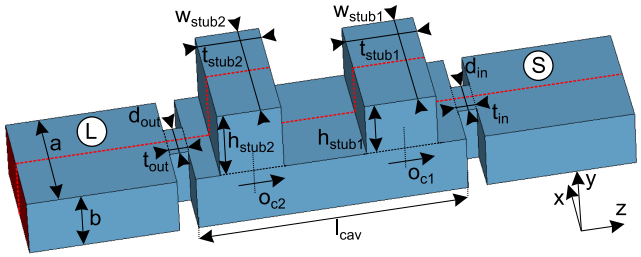

FIGURE 13. Triple-resonance filter consisting of a main TE_{102} mode cavity with length l_{cav} and two E-plane stubs. The red (dashed) line indicates the cutting plane.

The measurement takes places using a R&S ZVA67 network analyzer with ZC170 mm wave frequency converters after thru-reflect-line calibration using the commercial available calibration kit for the D-band [35]. The S-Parameters resulting from the coupling matrix representation with respect to the topology in Fig. 6(b) are shown in Fig. 12 as well and reveal good agreement to both, simulation and measurement. Deviations in the stopband might arise due to lower/higher order modes and dispersive effects of the waveguide building blocks, which are not included in the coupling matrix theory. The coupling factors are given in the caption of Fig. 12 and are found through an optimization based process.

III. TRIPLE-RESONANCE SEGMENT

A. BASIC CONSIDERATIONS

The basic dual-resonance segment from Fig. 1 can be extended to a triple-resonance element as shown in Fig. 13. It consists of a TE_{102} mode cavity as a base with two E-plane TM_{110} mode stubs placed on top of it. The TE_{102} mode cavity is coupled by inductive irises with diameter d_{in} / d_{out} to the source / load port, respectively. Initially, the first / second stub is placed at a quarter of l_{cav} away from the edges of the base cavity, but may have an offset denoted as o_{c1} / o_{c2}. The distance between the stubs center is therefore approximately half a wavelength. Both stubs are characterized by the height h_{stub}, the thickness t_{stub} as well as the width w_{stub}.

An S-Parameter simulation of the resonator in Fig. 13 with weak excitation ($d_{in} = d_{out} = 0.5$ mm) is shown in Fig. 14, while all other dimensions leading to this result are given in the caption. Three resonances as well as two TZs appear. The position of the upper TZ at 121.32 GHz can mainly be controlled by the height of the first stub h_{stub1}, while the height of the second stub can be used to control the position of the lower TZ at 112.28 GHz. However, also the resonance frequencies decrease by increasing the stubs height. This effect might be compensated by the other tuning means such as the width, thickness or offset position of the stubs from the center position. As there are no coupling elements within the triple-resonance element, the most suitable coupling topology is a transversal array of third order as shown in the inset of Fig. 14. The coupling matrix for defined specifications can be calculated as discussed in [29]. The electric field distribution of the resonating modes is shown in Fig. 14 as well.

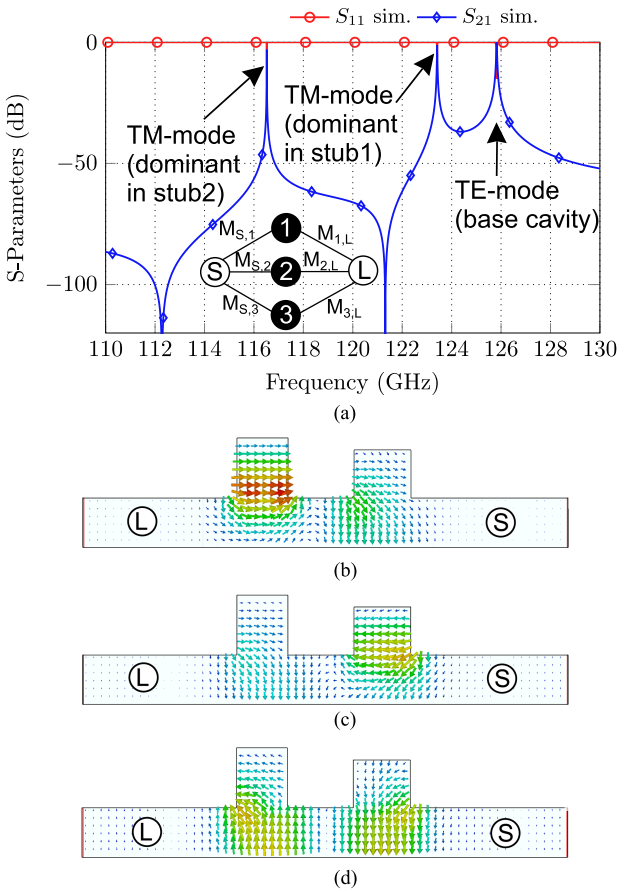

FIGURE 14. (a) S-Parameter simulation of the resonator in Fig. 13 with asymmetric stub arrangement and weak excitation. The inset shows the coupling topology. (b)-(d): Electric field distribution at resonance frequencies. The dimensions are as follows (all in mm): $d_{in} = d_{out} = 0.5$, $t_{in} = t_{out} = 0.25$, $l_{cav} = 3.6$, $h_{stub1} = 0.8$, $h_{stub2} = 1$, $t_{stub1} = 0.95$, $t_{stub2} = 0.85$, $w_{stub1} = w_{stub2} = a$, $o_{c1} = 0.05$, $o_{c2} = -0.15$.

The resonating modes might be identified more reliably by using a symmetrical model. The parameters (in agreement with Fig. 13) are choosen to be $h_{stub1} = h_{stub2} = 0.9$ mm, furthermore, there is no offset from the center position and the thickness of both stubs is $t_{stub1} = t_{stub2} = 0.9$ mm. In this symmetrical set-up, the modes in both stubs reveal an even / odd mode symmetry with respect to the center line as shown in Fig. 15(a) and (b), respectively. The mode in (c) is similar to the commonly known TE_{102} mode, while there are also field portions in both stubs. The modes might be interpreted as global eigenmodes of the overall structure [36] which can be excited from the source / load port, leading to the transversal array coupling matrix topology in Fig. 14 as proposed above.

Different options for tuning the resonance frequencies and finally obtaining a filter response are available. A parameter study which reveals the influence of the main design variables on the resonance frequencies and TZ positions is shown in Fig. 16. The study is based on the asymmetric set-up from Fig. 14. The TE_{102} mode can be associated with the green (diamond marked) line in Fig. 16(a) and is mostly effected by the cavity length l_{cav}. However, an influence of this parameter

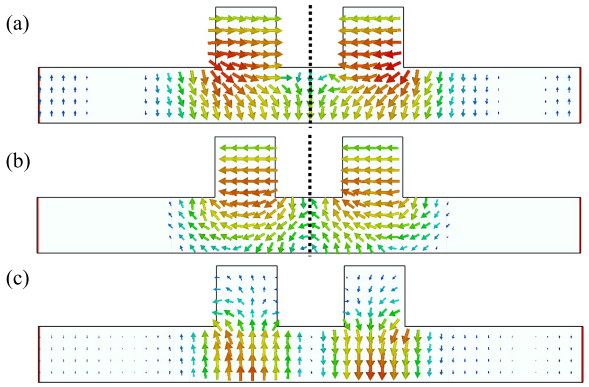

FIGURE 15. (a) / (b) Electric field distribution of the even (open circuit) / odd (short circuit) modes, respectively, and (c) electric field of TE_{102} mode. The dashed lines visualize the symmetry plane. The field evaluation takes place with a symmetric stub arrangement.

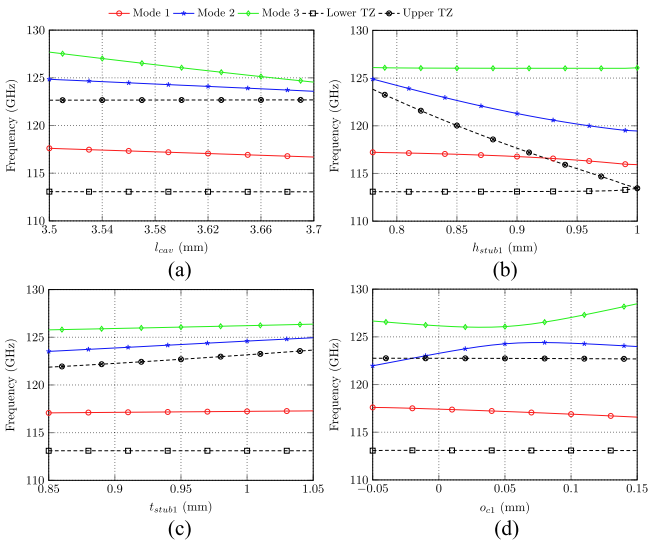

FIGURE 16. Frequency of the resonant modes and TZs in dependency from the geometric dimensions: (a) length of base cavity l_{cav}, (b) height of first stub h_{stub1}, (c) thickness of first stub t_{stub1} and (d) offset of the first stub from center position o_{c1}. For this study the initial dimensions as in Fig. 14 (asymmetric arrangement) are used.

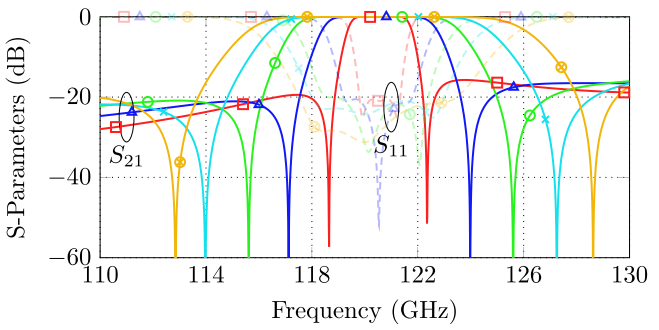

FIGURE 17. Bandwidth study of the third order filter as shown in Fig. 13. The bandwidth is varied between 1.4 GHz ($FBW = 1.16\%$) and 6 GHz ($FBW \approx 5\%$) while maintaining a constant center frequency and relative TZ positions.

on both stub modes is obvious as well. The blue (star marked) line exhibits similarity with the even mode from Fig. 15(a), where a significant field portion is concentrated in the first stub due to the de-tuning from the ideal symmetric configuration. The red (circle marked) line has similarity with the odd mode from Fig. 15(b) with a dominant field portion in the second stub. The TZ positions (dashed black lines) are completely unaffected by l_{cav}. The height of the first stub is varied in Fig. 16(b). On the one hand, the blue (star marked) curve representing the even mode decreases with increasing stub height. As already mentioned, a significant field portion of this mode is concentrated in the first stub due to the unequal tuning in comparison to the case discussed in Fig. 15. On the other hand, the TZ associated with this stub decreases in frequency as well. The red (circle marked) curve is also slightly de-tuned in frequency. By increasing the thickness of the first stub t_{stub1} in Fig. 16(c), an increase of both the resonance frequency as well as the TZ associated with the first stub is remarked. The TE_{102} mode is slightly increased by this operation as well (green, diamond marked line). Finally, in Fig. 16(d) the results of varying the offset of the first stub from the center position are presented. As an important result for negative values of o_{c1}, it is possible to exchange the relative position of a resonance and the upper TZ, as required for the realization of a passband in the filter design process. Additionally, the mode designation changes and more diverges from the symmetric case discussed in Fig. 15.

As in the case of the realization of fourth and higher-order filters in Section II, multiple cross-dependencies exist and prevent the application of a straight-forward filter synthesis strategy. The triple-resonance filter is therefore manually pre-tuned in compliance with Fig. 16 by adjusting all resonances to be close to the desired center frequency utilizing a realistic input / output coupling strength (d_{in} / d_{out}). The structure is subsequently optimized to the desired specifications (bandwidth, TZ positions, RL level).

Like the coupled fourth order filter, the triple-resonance segment reveals a high flexibility in terms of bandwidth and TZ positioning. Fig. 17 shows a study, where the bandwidth is increased from 1.4 GHz ($FBW = 1.16\%$) to 6 GHz ($FBW \approx 5\%$) by maintaining a constant center frequency of 120.5 GHz as well as constant relative TZ positions at $f_{TZ,LP} = \pm j2.63$. As design guideline, it must be considered to increase d_{in} and d_{out} for increasing bandwidths while l_{cav} decreases. As the absolute position of both TZs diverges for increasing bandwidths, the associated stub heights change as well. Particularly, h_{stub1} decreases while h_{stub2} increases for larger bandwidths, which agrees well with the result from Fig. 16(b). Finally, it must be mentioned that the stubs thickness varies in the optimization process and for extreme small / wide bandwidths dimensions might result, which are unpractical for fabrication.

Similarly, it is possible to shift e.g. the lower TZ by maintaining a constant filter characteristic as it is shown in Fig. 18. The TZ is moved from 118.4 GHz ($f_{TZ,LP} = -j1.41$) to

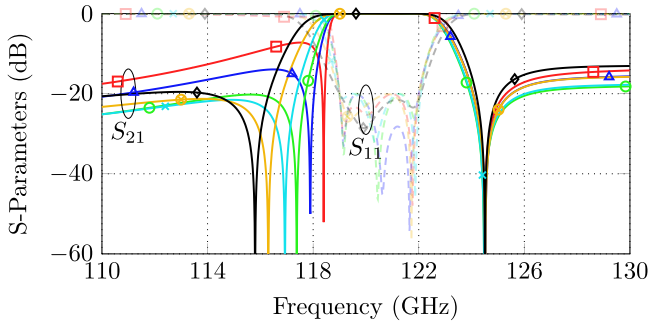

FIGURE 18. Flexibility of the lower TZ of the third order filter as shown in Fig. 13. The TZ is varied on the normalized frequency axis between $f_{TZ,LP} = -j1.41$ and $f_{TZ,LP} = -j3.19$.

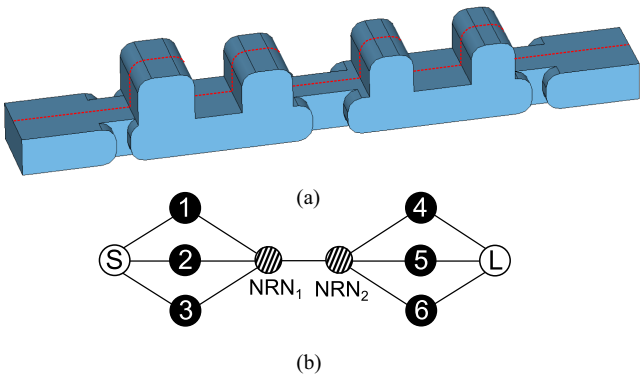

FIGURE 19. (a) Simulation model of a sixth order filter consisting of two coupled triple-resonance segments and (b) coupling topology.

115.8 GHz ($f_{TZ,LP} = -j3.19$) by maintaining a constant center frequency of 120.5 GHz and bandwidth of 3 GHz. The upper TZ is fixed as well at 124.5 GHz ($f_{TZ,LP} \approx j2.62$).

B. HIGHER ORDER FILTERS BASED ON THE TRIPLE-RESONANCE SEGMENT

Different options for the realization of higher order filters are available. Either several triple-resonance sections can be coupled or even a combination with TE_{101} mode cavities as well as dual-resonance segments from Sections II-A can take place. This section describes the achievable filter responses by combining two third order segments as shown in Fig. 13. The simulation model as well as the proposed topology are shown in Fig. 19(a) and (b), respectively. The coupling between both triple-resonance segments takes place by an inverter which is modeled in the topology as two consecutive NRNs coupled by a unity inverter. As expected from the discussion of the former section, four TZs on the real frequency axis, which can be flipped to positions above or below the passband, are generated by this structure. The flexibility of flipping the TZs is demonstrated in Fig. 20, where three configurations are shown. Apart from the case in which two TZs are placed above and below the passband, either three or even four TZs can be placed above the passband. Especially the latter case might be valuable for practical implementations, where e.g. highly asymmetric rejection specifications should be realized

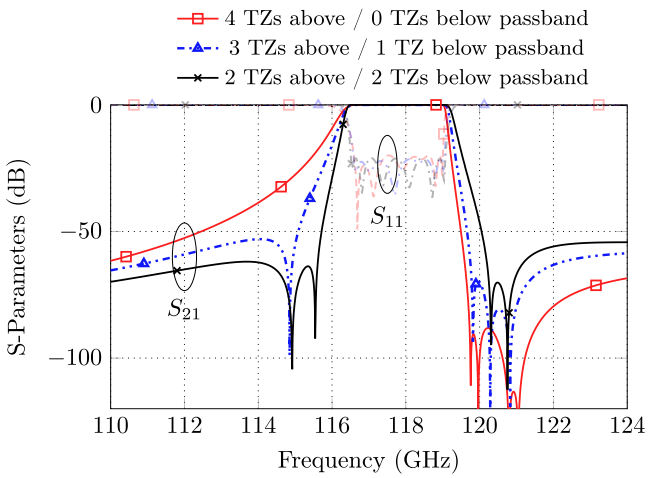

FIGURE 20. Flexibility of the proposed sixth order filter from Fig. 19(a) with respect to the TZ positioning.

with an easy manufacturable filter. It is worth mentioning that the simulation model in Fig. 19(a) can still be cut along the E-plane for manufacturing purposes into two identical halves while structures that are difficult to realize are avoided. A prototype is manufactured and the results are discussed in Sections III-C in order to verify the good machining properties. The presented simulation results from Fig. 20 reveal a constant center frequency of 117.8 GHz and a bandwidth of 2.4 GHz.

C. MEASUREMENT RESULTS

The filter model generating the S-Parameter response from Fig. 20, where three TZs are placed above the passband and one TZ is below the passband, is manufactured as proof of concept. The filter model with all radii required for the manufacturing is shown in Fig. 19(a). The fabrication and measurement takes place under the same conditions as discussed in Section II-C. The measurement results in comparison to the simulation are shown in Fig. 21. The manufactured prototype is matched to a return loss level of approx. 18.5 dB while no significant change in the transmission characteristic is noticeable. The unloaded Q-factor can be estimated to $Q_u \approx 980$. It should be mentioned that, as in the case of the first filter, the prototype is manufactured from brass and no surface treatment is applied. The Q-factor might be further increased by applying a thin gold or silver layer. Sputtering is particularly suitable in this case, because the filter geometry does not have a high aspect ratio.

IV. QUADRUPLE-RESONANCE SEGMENT

A. BASIC CONSIDERATIONS

The last building block proposed within this paper is a quadruple-resonance segment. In many practical applications a fourth order stand-alone filter might be sufficient to fulfill the desired specifications. Two options are available for this scenario: either the coupled fourth order filter investigated in Sections II-B can be used while otherwise an extension

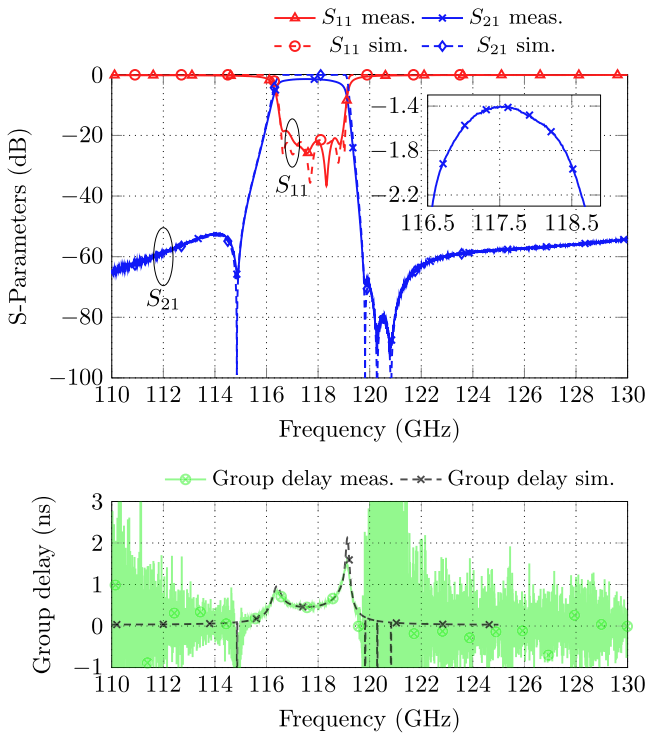

FIGURE 21. Top: Measured S-Parameters in comparison to the simulation of the filter prototype in Fig. 19(a). Bottom: Comparison of measured and simulated group delay.

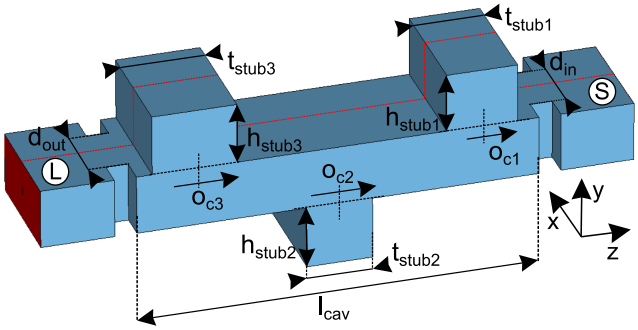

FIGURE 22. Quadruple-resonance element consisting of a main TE_{103} mode cavity with length l_{cav} and three E-plane stubs. The red (dashed) line indicates the cutting plane.

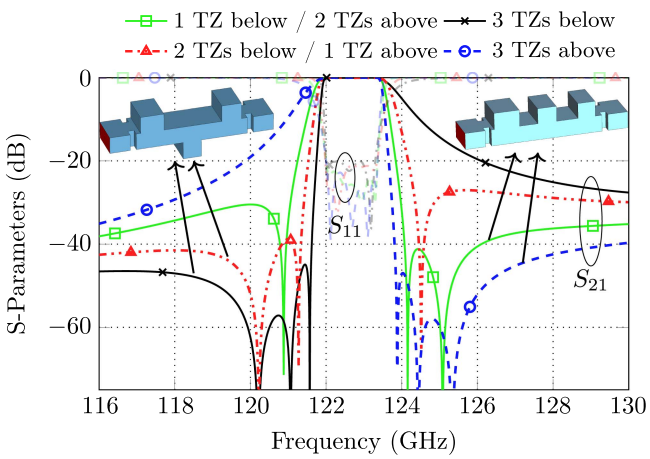

FIGURE 23. Flexibility of the proposed fourth order quadruple-resonance filter with respect to the TZ positioning. The insets show the simulation models.

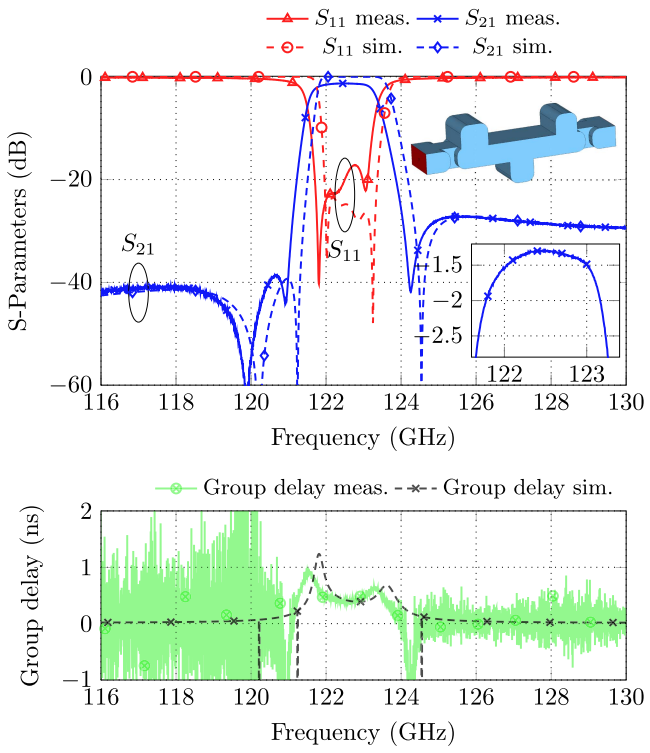

FIGURE 24. Top: Measured S-Parameters in comparison to the simulation. The inset shows the simulation model with all required radii. Bottom: Comparison of measured and simulated group delay.

of the triple-resonance segment into a quadruple-resonance element is possible as well. As an advantage of the second option, three TZs near to the passband are available which reveal, otherwise, limited flexibility. The basic structure is shown in Fig. 22 and consists of a base TE_{103} mode resonator with length l_{cav} coupled by inductive irises with diameter d_{in} and d_{out}. In total three E-plane TM mode stubs are placed along the base resonator. The first / last stub is initially placed with $l_{cav}/8$ distance from the in-/ output coupling iris of the TE_{103} mode cavity and may have an offset denoted as o_{c1} / o_{c3}, respectively. The middle stub is placed at $l_{cav}/2$ and may has an offset as well which is denoted as o_{c2}. In Fig. 22, the first and third stub extends in positive y-direction while the middle one is directed in the opposite direction. The alternating arrangement of the stubs in not necessarily required but reveals advantageous rejection properties if at least two of the available TZs are placed below the passband. It is interesting to observe that even other configurations with respect to the stubs direction may result in a matched filter response. However, in some configurations at least two TZs are inseparable combined with each other.

Under the defined design constraints, the prototype shows small flexibility as e.g. the TZ positions are nearly fixed for a given configuration. In the study of Fig. 23 two different

TABLE 1. Comparison With Recently Published Works (Where f_0 Is the Center Frequency, *FBW* Is the Fractional Bandwidth, *n* Is the Filter Order, TZs Is the Number of TZs, *RL* the Maximal Return Loss in the Passband and *IL* the Minimal Insertion Loss in the Passband)

Ref.	Year	Type	Manufacturing Techn.	f_0 (GHz)	FBW (%)	n	TZs	RL (dB)	IL (dB)
[37]	2022	Filter	E-Plane waveguide filter	88.55	3.6 (3-dB)	2	3	18	1.15
[38]	2016	Filter	CNC, H-plane, aluminum	92.65	5.5 (3-dB)	4	4	15	1.2 (average)
[39]	2019	Filter	CNC, H-plane, aluminum	92.5	20.2 (3-dB)	5	1	15	0.6 (average)
[40]	2013	Filter	CNC, E-plane, brass	99.5	5	4	0	25	0.7
[41]	2018	Filter	Silicon micromachining, gold plating	140	8.6	6	0	16*	0.41
[42]	2020	Filter	CNC, gold plating	140	17.18 (3-dB)	8	3	12.5	0.33
[43]	2022	Filter	Structured glass, gold plating	87.86	2.3	4	0	22	1.43
T. W. (filter 1)	2022	Filter	CNC, E-Plane cut, brass	117.15	3.38	4	2	22	0.5
T. W. (filter 2)	2022	Filter	CNC, E-Plane cut, brass	117.76	2.16	6	4	18.5	1.44
T. W. (filter 3)	2022	Filter	CNC, E-Plane cut, brass	122.41	1.15	4	3	17.15	1.3

configurations are investigated. The prototypes generating two or even three TZs below the passband have the same structure as shown in Fig. 22. Otherwise, if two or even all available TZs are flipped to the upper passband side, the prototype with all-equal stub directions reveals a superior performance. It must be mentioned that even the basic prototype in Fig. 22 allows that two or three TZs are placed above the passband. However, these TZs are either very close or even combined with each other. The possibility to flip individual stubs up or down increases the degrees of freedom in the design process and especially allows to fulfill asymmetric attenuation requirements. Within this study, the prototypes have a center frequency of approx. 122.65 GHz and bandwidths between 1.3 GHz and 1.35 GHz. Finally, it should be mentioned that a combination with further TE_{101} mode cavities can take place to e.g. increase the filter order.

B. MEASUREMENT RESULTS

In order to verify the good manufacturing qualities, a fourth order filter is manufactured. The filter is designed to have two TZs below and one TZ above the passband. The band edges are located at $f_l = 122$ GHz and $f_u = 123.3$ GHz ($FBW = 1.06\%$). The measurement results are compared to the simulation in Fig. 24. The manufactured prototype reveals a return loss level of at least 17.2 dB and has an unloaded Q-factor of $Q_u \approx 1000$. Furthermore, a 320 MHz (0.26%) downshift of the center frequency appears due to manufacturing inaccuracies.

V. COMPARISON

Table 1 compares the results obtained within this work with results of filters from the literature in a similar frequency range. All three filters realized and characterized within this work are compared with respect to the following aspects: type of component, manufacturing technology, center frequency f_0 (GHz), fractional bandwidth FBW (%), filter order n, number of TZs, maximal return loss level in the passband as well as minimal insertion loss level in the passband. If some of the parameters are not explicitly stated in the corresponding paper, these values are estimated and noted with a star. If filters are manufactured using CNC milling, the cutting plane which is required for fabrication as well as a potential surface plating are mentioned.

VI. CONCLUSION

In this paper, multi-resonance stub-based building blocks with low manufacturing complexity especially suitable for waveguide filters in the mm-Wave frequency range are presented. All components feature an E-plane symmetry, which ease the manufacturing and increase the achievable unloaded quality factor. Dual-, triple- as well as quadruple-resonance sections are presented as a kind of building block, revealing between one and three TZs. A high design flexibility (TZ positions, bandwidth) can directly be achieved by the cascaded dual-resonance fourth order filter or by the triple-resonance segment. If higher order filters are required, a combination of different building blocks can be considered for the realization of the desired specifications. Three quasi-elliptical filters with good agreement to the simulation were manufactured as proof of concept, revealing the advantageous manufacturing qualities of the proposed filters in the D-band. Due to the mechanical E-plane cut, unloaded quality factors in the range between 830 and 1000 were obtained by using brass material without any additional surface treatment. The Q-factors might be further increased by sputtering a gold or silver layer, which is especially convenient as no high aspect ratios are present in the filter geometries. Finally, due to the good fabrication properties, these filters might be further downscaled to higher frequency bands.

REFERENCES

[1] E. López-Oliver and C. Tomassoni, "3-D-printed dual-mode filter using an ellipsoidal cavity with asymmetric responses," *IEEE Microw. Wireless Compon. Lett.*, vol. 31, no. 6, pp. 670–673, Jun. 2021.

[2] J. A. Lorente, M. M. Mendoza, A. Z. Petersson, L. Pambaguian, A. A. Melcon, and C. Ernst, "Single part microwave filters made from selective laser melting," in *Proc. Eur. Microw. Conf.*, 2009, pp. 1421–1424.

[3] S. Liu, J. Hu, Z. Xuan, Y. Zhang, and R. Xu, "Micromachined WR-1.0 waveguide band-pass filter," in *Proc. IEEE Int. Conf. Microw. Millimeter Wave Technol.*, Beijing, China, 2016, pp. 949–951.

[4] X. Shang et al., "Submillimeter-wave waveguide filters fabricated by SU-8 process and laser micromachining," *IET Microw. Antennas Propag.*, vol. 11, no. 14, pp. 2027–2034, Oct. 2017.

[5] S. Liu et al., "1 THz micromachined waveguide band-pass filter," *J. Infrared, Millimeter, THz Waves*, vol. 37, no. 5, pp. 435–447, Dec. 2015.
[6] O. Glubokov, X. Zhao, B. Beuerle, J. Campion, U. Shah, and J. Oberhammer, "Micromachined multilayer bandpass filter at 270 GHz using dual-mode circular cavities," in *Proc. IEEE MTT-S Int. Microw. Symp.*, Honololu, HI, USA, 2017, pp. 1449–1452.
[7] O. Glubokov, X. Zhao, J. Campion, U. Shah, and J. Oberhammer, "Micromachined filters at 450 GHz with 1% fractional bandwidth and unloaded Q beyond 700," *IEEE Trans. THz Sci. Technol.*, vol. 9, no. 1, pp. 106–108, Jan. 2019.
[8] O. Glubokov, X. Zhao, J. Campion, U. Shah, and J. Oberhammer, "Micromachined bandpass filters with enhanced stopband performance and Q-factor of 950 at 700 GHz," in *Proc. IEEE MTT-S Int. Microw. Symp.*, Atlanta, GA, USA, 2021, pp. 204–206.
[9] X. Shang, Y. Tian, M. J. Lancaster, and S. Singh, "A SU8 micromachined WR-1.5 band waveguide filter," *IEEE Microw. Wireless Compon. Lett.*, vol. 23, no. 6, pp. 300–302, Jun. 2013.
[10] Q. Chen, M. Lancaster, J. Xu, Y. Tian, and X. Shang, "SU-8 micromachined WR-3 band waveguide bandpass filter with low insertion loss," *Electron. Lett.*, vol. 49, no. 7, pp. 480–482, Mar. 2013.
[11] H. Yang et al., "WR-3 waveguide bandpass filters fabricated using high precision CNC machining and SU-8 photoresist technology," *IEEE Trans. THz Sci. Technol.*, vol. 8, no. 1, pp. 100–107, Jan. 2018.
[12] V. Furtula and M. Salewski, "W-band waveguide bandpass filter with E-plane cut," *Rev. Sci. Instrum.*, vol. 85, no. 7, Jul. 2014, Art. no. 074703.
[13] N. Zhang, R. Song, M. Hu, G. Shan, C. Wang, and J. Yang, "A low-loss design of bandpass filter at the terahertz band," *IEEE Microw. Wireless Compon. Lett.*, vol. 28, no. 7, pp. 573–575, Jul. 2018.
[14] D. Koller, E. W. Bryerton, and J. L. Hesler, "WM380 (675-700 GHz) bandpass filters in milled, split-block construction," *IEEE Trans. THz Sci. Technol.*, vol. 8, no. 6, pp. 630–637, Nov. 2018.
[15] J.-Q. Ding, S.-C. Shi, K. Zhou, Y. Zhao, D. Liu, and W. Wu, "WR-3 band quasi-elliptical waveguide filters using higher order mode resonances," *IEEE Trans. THz Sci. Technol.*, vol. 7, no. 3, pp. 302–309, May 2017.
[16] J.-Q. Ding, S.-C. Shi, K. Zhou, D. Liu, and W. Wu, "Analysis of 220-GHz low-loss quasi-elliptic waveguide bandpass filter," *IEEE Microw. Wireless Compon. Lett.*, vol. 27, no. 7, pp. 648–650, Jul. 2017.
[17] Y. Xiao, P. Shan, K. Zhu, H. Sun, and F. Yang, "Analysis of a novel singlet and its application in THz bandpass filter design," *IEEE Trans. THz Sci. Technol.*, vol. 8, no. 3, pp. 312–320, May 2018.
[18] C. A. Leal-Sevillano, J. R. Montejo-Garai, J. A. Ruiz-Cruz, and J. M. Rebollar, "Low-loss elliptical response filter at 100 GHz," *IEEE Microw. Wireless Compon. Lett.*, vol. 22, no. 9, pp. 459–461, Sep. 2012.
[19] U. Rosenberg, S. Amari, and J. Bornemann, "Inline TM_{110}-mode filters with high-design flexibility by utilizing bypass couplings of nonresonating $TE_{10/01}$ modes," *IEEE Trans. Microw. Theory Techn.*, vol. 51, no. 6, pp. 1735–1742, Jun. 2003.
[20] S. Amari, U. Rosenberg, and J. Bornemann, "Singlets, cascaded singlets, and the nonresonating node model for advanced modular design of elliptic filters," *IEEE Microw. Wireless Compon. Lett.*, vol. 14, no. 5, pp. 237–239, May 2004.
[21] S. Bastioli, "Nonresonating mode waveguide filters," *IEEE Microw. Mag.*, vol. 12, no. 6, pp. 77–86, Oct. 2011.
[22] D. Miek, F. Kamrath, P. Boe, and M. Höft, "T-shaped dual-mode waveguide filters with low manufacturing complexity for mm-Wave applications," in *Proc. IEEE MTT-S Int. Microw. Filter Workshop*, 2021, pp. 1–3.
[23] S. Bastioli and R. V. Snyder, "The stubbed waveguide cavity," in *Proc. IEEE MTT-S Int. Microw. Symp.*, Boston, MA, USA, 2019, pp. 1187–1189.
[24] S. Bastioli and R. V. Snyder, "Stubbed waveguide cavity filters," *IEEE Trans. Microw. Theory Techn.*, vol. 67, no. 12, pp. 5049–5060, Dec. 2019.
[25] S. Bastioli and R. V. Snyder, "New triple-resonance configuration using stubbed waveguide dual-mode cavities," *IEEE Microw. Wireless Compon. Lett.*, vol. 32, no. 6, pp. 652–655, Jun. 2022.
[26] S. Amari and J. Bornemann, "Using frequency-dependent coupling to generate finite attenuation poles in direct-coupled resonator bandpass filters," *IEEE Microw. Guided Wave Lett.*, vol. 9, no. 10, pp. 404–406, Oct. 1999.
[27] J. Bornemann and J. Uher, "H-plane waveguide filters with E-plane dispersive inverters for high-power applications," in *Proc. 10th Int. Symp. Antenna Technol. Appl. Electromagn. URSI Conf*, 2004, pp. 1–4.
[28] Q. Wang and J. Bornemann, "Synthesis and design of direct-coupled rectangular waveguide filters with arbitrary inverter sequence," in *Proc. 16th Int. Symp. Antenna Techn. Appl. Electromagn.*, 2014, pp. 1–6.
[29] R. J. Cameron, "Advanced coupling matrix synthesis techniques for microwave filters," *IEEE Trans. Microw. Theory Techn.*, vol. 51, no. 1, pp. 1–10, Jan. 2003.
[30] U. Rosenberg and S. Amari, "Novel coupling schemes for microwave resonator filters," *IEEE Trans. Microw. Theory Techn.*, vol. 50, no. 12, pp. 2896–2902, Dec. 2002.
[31] C. Bartlett, J. Bornemann, and M. Höft, "3-D-printing and high-precision milling of W-band filter components with admittance inverter sequences," *IEEE Trans. Compon. Packag. Manuf. Technol.*, vol. 11, no. 12, pp. 2140–2147, Dec. 2021.
[32] S. Amari and U. Rosenberg, "Design of dual-mode bandpass waveguide elliptic filters for simple fabrication by milling," *Int. J. RF Microw. Comput. Aided Eng.*, vol. 17, no. 1, pp. 34–40, Jan. 2007.
[33] S. Amari and U. Rosenberg, "New building blocks for modular design of elliptic and self-equalized filters," *IEEE Trans. Microw. Theory Techn.*, vol. 52, no. 2, pp. 721–736, Feb. 2004.
[34] G. Macchiarella, "Extraction of unloaded Q and coupling matrix from measurements on filters with large losses," *IEEE Microw. Wireless Compon. Lett.*, vol. 20, no. 6, pp. 307–309, Jun. 2010.
[35] M. Hiebel, "Multiport millimeter-wave measurements using converters of the R&S ZVA-family," Application note 1EZ56, Rohde & Schwarz, pp. 1–24, Sep. 2007. [Online]. Available: https://scdn.rohde-schwarz.com/ur/pws/dl_downloads/dl_application/application_notes/1ez56/1EZ56_0E.pdf
[36] S. Amari and M. Bekheit, "Physical interpretation and implications of similarity transformations in coupled resonator filter design," *IEEE Trans. Microw. Theory Techn.*, vol. 55, no. 6, pp. 1139–1153, Jun. 2007.
[37] Y. Jiang et al., "W-band E-plane waveguide filter using compact beeline resonator," *IEEE Microw. Wireless Compon. Lett.*, vol. 32, no. 4, pp. 289–292, Apr. 2022.
[38] J. Ding, D. Liu, S. Shi, and W. Wu, "W-band quasi-elliptical waveguide filter with cross-coupling and source-load coupling," *Electron. Lett.*, vol. 52, no. 23, pp. 1960–1961, Nov. 2016.
[39] J. Xu, J.-Q. Ding, Y. Zhao, and J.-X. Ge, "W-band broadband waveguide filter based on H-plane offset coupling," *J. Infrared, Millimeter, THz Waves*, vol. 40, no. 4, pp. 412–418, Feb. 2019.
[40] C. A. Leal-Sevillano, J. R. Montejo-Garai, J. A. Ruiz-Cruz, and J. M. Rebollar, "Experimental comparison of waveguide filters at W-band implemented by different machining processes and split-block," *J. Electromagn. Waves Appl.*, vol. 27, no. 18, pp. 2390–2394, 2013.
[41] J. Campion et al., "An ultra low-loss silicon-micromachined waveguide filter for D-band telecommunication applications," in *Proc. IEEE/MTT-S Int. Microw. Symp.*, Philadelphia, PA, USA, 2018, pp. 583–586.
[42] Y.-W. Wu, Z.-C. Hao, R. Lu, and J.-S. Hong, "A high-selectivity D-band mixed-mode filter based on the coupled overmode cavities," *IEEE Trans. Microw. Theory Techn.*, vol. 68, no. 6, pp. 2331–2342, Jun. 2020.
[43] C. Bartlett, A. Malave, M. Letz, and M. Höft, "Structured-glass waveguide technology for high-performance millimetre-wave components and systems," *IEEE J. Microwaves*, vol. 2, no. 2, pp. 307–315, Apr. 2022.

DANIEL MIEK (Member, IEEE) was born in Minden, Germany, on January 10, 1992. He received the B.Sc. and M.Sc. degrees in electrical engineering and information technology in 2015 and 2017, respectively, from Kiel University, Kiel, Germany, where he is currently working toward the Dr.-Ing. degree as a member with the Chair of Microwave Engineering, Department of Electrical and Information Engineering. His research interests include the design, realization and optimization of waveguide, and dielectric filters.

FYNN KAMRATH (Graduate Student Member, IEEE) received the B.Sc. and M.Sc. degrees in electrical engineering and information technology from Kiel University, Kiel, Germany, in 2017 and 2019, respectively, where he is currently working toward the Dr.-Ing. degree with the Chair of Microwave Engineering, Institute of Electrical Engineering and Information Technology. His research interests include the design, realization, and optimization of center frequency and bandwidth tunable microwave filters.

KENNET BRAASCH received the B.Sc. and M.Sc. degrees in electrical engineering and information technology from Kiel University, Kiel, Germany, in 2018 and 2020, respectively, where he is currently working toward the Dr.-Ing. degree as a member with the Chair of microwave Engineering, Institute of Electrical Engineering and Information Technology. His research interests include the design of a radar system for the detection and characterization of small particle streams.

PATRICK BOE (Graduate Student Member, IEEE) received the B.Sc. and M.Sc. degrees in electrical engineering, information technology, and business management from Kiel University, Kiel, Germany, in 2017 and 2019, respectively, where he is currently working toward the Dr.-Ing. degree as a member with the Chair of Microwave Engineering, Institute of Electrical Engineering and Information Technology. His research interests include the design, realization and optimization of dielectric resonator filters, and also dielectric multi-mode filters.

MICHAEL HÖFT (Senior Member, IEEE) was born in Lübeck, Germany, in 1972. He received the Dipl.-Ing. degree in electrical engineering and Dr.-Ing. degree from Hamburg University of Technology, Hamburg, Germany, in 1997 and 2002, respectively. From 2002 to 2013, he joined the Communications Laboratory, European Technology Center, Panasonic Industrial Devices Europe GmbH, Lüneburg, Germany. He was a Research Engineer and then Team Leader, where he was engaged with Research and Development of microwave circuitry and components, particularly filters for cellular radio communications. From 2010 to 2013, he was a Group Leader for Research and Development of sensor and network devices. Since October 2013, he has been a Full Professor with the Faculty of Engineering, Kiel University, Kiel, Germany, where he is currently the Head of the Microwave Group, Institute of Electrical and Information Engineering. His research interests include active and passive microwave components, (sub-) millimeter-wave quasi-optical techniques and circuitry, microwave and field measurement techniques, microwave filters, microwave sensors, as well as magnetic field sensors. Dr. Höft is a member of the European Microwave Association (EuMA), Association of German Engineers (VDI), and the German Institute of Electrical Engineers (VDE).